Journal of the European Ceramic Society **11** (1993) 161–170

Characterisation of Chemically Prepared ZnO Powders in Relation to the Nonlinear Resistors

T. R. N. Kutty & N. Raghu

Materials Research Centre, Indian Institute of Science, Bangalore 560012, India

(Received 6 January 1992; revised version received 6 April 1992; accepted 3 July 1992)

Abstract

ZnO powders prepared from the thermal decomposition of Zn-oxalate, Zn-carbonate and Zn-nitrate have been characterised in relation to the formation of sintered ceramics exhibiting nonlinear resistivity. The particle characteristics such as size, shape, lattice strain, the point defect contents and the nonstoichiometry with respect to δ_{Zn} value in $Zn_{1+\delta}O$ are found to depend upon the mechanism of reactions of ZnO formation and the effect of back reaction from the evolved gases. The most important characteristic of ZnO powder that considerably influences the nonlinear property of the ceramics is δ_{Zn}. Optimum current–voltage characteristics for the sintered products are obtained when δ_{Zn} in the starting material is in the range 8·5–12 ppma. Because of nonstoichiometry, the native donor states are built in the powder particles. The depletion layers formed at the pre-sintering stage are retained during sintering, as a result of the high valent transition metal ions preferentially present at the grain boundary regions. The energy barriers are stabilised around the grain boundaries by this process.

ZnO-Pulver, die mittels thermischer Zersetzung von Zn-Oxalat, Zn-Karbonat und Zn-Nitrat hergestellt wurden, sind im Zusammenhang mit der Bildung gesinterter Keramiken, die ein nicht-lineares Widerstandsverhalten aufweisen, charakterisiert worden. Es wurde festgestellt, daß Teilcheneigenschaften, wie Größe, Form, Gitteraufdehnung, Konzentration punktförmiger Defekte und die Nichtstöchiometrie in Bezug auf den δ_{Zn}-Wert in $Zn_{1+\delta}O$ von den Reaktionsmechanismen der ZnO-Bildung und von der Auswirkung der Rückreaktion der entwickelten Gase abhängen Diebedeutendste Eigenschaft des untersuchten ZnO-Pulvers, die beträchtlichen Einfluß auf die nicht-linearen Eigenschaften der Keramiken ausübt, ist δ_{Zn}. Optimale Strom Spannungskennlinien der gesinterten Werkstoffe werden erreicht, wenn δ_{Zn} des Ausgangsmaterials im Bereich zwischen 8·5 und 12 ppma liegt. Aufgrund der Nichtstöchiometrie entstehen die ursprünglichen Donatorzustände in den Pulverteilchen. Erschöpfte Schichten, die im Stadium des Vorsinterns gebildet werden, bleiben während des Sinterns erhalten, weil die hochvalenten Übergangsmetallionen vorzugsweise in den Korngrenzenbereichen angesiedelt sind. Durch diesen Prozeß werden die Energiebarrieren im Bereich der Korngrenzen stabilisiert.

Des poudres de ZnO, produites par décomposition thermique d'oxalate de Zn, carbonate de Zn et nitrate de Zn ont été characterisées pour préparer des céramiques frittées présentant une résistivité non linéaire. Les caractéristiques des particules telles que leur taille, leur morphologie ainsi que la déformation du réseau, la teneur en défauts ponctuels et la non stoechiométrie exprimée selon la valeur de δ_{Zn} dans $Zn_{1+\delta}O$, semblent dépendre du mécanisme de la réaction de formation de ZnO ainsi que de la réaction en retour des gaz émis. La caractéristique la plus importante, en se qui concerne les propriétés de non linéarité, est la valeur de δ_{Zn}. Les caractéristiques optimales courant–tension du produit fritté sont obtenues quand la composition initiale exprimée en δ_{Zn} vaut de 8·5 à 12 ppma. En raison de la non stoechiométrie, les états donneurs natifs existent dans la poudre. Les couches de déplétion formées dans l'étape de pré-frittage sont conservées pendant le frittage car les ions de mataux de transition à valence élevée se localisent préférentiellement aux joints de grains. Ce processus stabilise les barrières d'énergie autour des joints de grains.

1 Introduction

It is well known that purity, particle size, shape, microstrain, native point defect concentration and reactivity of the starting powders play a major role

Journal of the European Ceramic Society 0955-2219/93/$6.00

in the performance of the final ceramics. Commercially available ZnO powders of analytical grade purity are found to yield ceramics of low nonlinearity coefficients, irrespective of the forming additives used. ZnO is produced in large quantities by burning the zinc ores (mostly sulphides) or Zn vapour in air.[1-4] However, reactive ZnO powders with controlled particle size have been prepared by the wet chemical methods.[5-8] Many reports exist on the preparation of pure ZnO through the alkoxide route as well as by other methods.[9-12] Since wide variations in the nonlinear property were observed for different ZnO starting materials, for the present study the authors undertook a systematic investigation on the chemically prepared ZnO powders in relation to the formation of ceramics exhibiting prominent varistor characteristics. Three different chemical routes were adopted, namely the thermal decomposition of the oxalate, carbonate or nitrates of Zn, wherein the purpose was to analyse the influence of the mode of formation on the nature of the powder. As-prepared or heat-treated powders from these three routes have been made use of in preparing the varistor ceramics with suitable additives. It is found that higher nonlinearity coefficients are obtained only under a specific range of nonstoichiometric values for the starting powders and that the critical defect contents are better correlatable to nonlinearity than to particle size.

2 Experimental Section

2.1 Preparation of the ZnO powders

Purification of the starting material was found to be an essential step. $ZnCl_2$ was prepared by dissolving Zn granules (analytical grade) in high purity HCl and was retained in a column containing Zn-granules for 24 h. This served to deposit any impurities that were more electropositive than Zn. After draining the solution, the surface of the Zn granules was thoroughly cleaned with dilute HCl. The $ZnCl_2$ solution was returned to the column. These steps were carried out 4–6 times.[13] The transition metal impurities had been removed by the fractional precipitation technique. Advantage was taken of the fact that the impurities get preferentially accumulated in the early formed precipitate. The final precipitation was carried out at pH ~ 8. This precipitate was thoroughly washed several times with slightly ammoniacal double distilled water and the removal of possible traces of chloride had been confirmed by the silver nitrate test. The filtered precipitate was dried in an oven at 100°C for 2 h. Ultrafine ZnO powder was obtained by decomposing $Zn_2(OH)_2CO_3$ at 300–500°C for 4 h.[7] $ZnC_2O_4 . H_2O$ and $Zn_3(OH)_4(NO_3)_2$ were prepared as described in Refs 6 and 8, respectively. These precursors were decomposed under controlled conditions and were further annealed at higher temperatures. For the sake of convenience, ZnO powders prepared under different conditions are designated as given in Table 1. The impurity contents in ZnO prepared from the above precursors were: Cd = 2, Cu = 0·1, Mn = 12, Mg = 3, Ca = 0·5, Na = 0·1, Sn = 0·5, K = 0·2, Pb = 3, Cl = 16 (all in ppm; analyses by ICP-AAS).

2.2 Methods of characterisation

X-ray powder patterns were recorded with a Philips 1700 diffractometer using cobalt K_α ($\lambda = 1{\cdot}7902$ Å) source, in a slow scan mode of 1/8° per minute on an extended scale so that $2\theta = 1°$ corresponds to 8 cm. The particle size and shape were measured using the Williamson–Hall method, assuming Cauchy as well as Gaussian distribution.[14] These results are further cross-checked using the Warren–Averbach method[15] with correction for the 'hook effect'. Annealing of the powders at different temperatures were carried out for 15 h. Preliminary investigations showed that the full width at half-maximum intensity of X-ray peaks were constant after 15 h of annealing. The K_α contribution was separated using Rachinger correction.[16] The instrumental line-broadening was corrected using quartz as the internal standard. The data were further corrected for polarisation, and the Lorentz factor and the background obtained by a procedure of least squares was subtracted. The particle size, morphology and the size distribution of the powders were analysed using optical (Leitz, Wetzlar, Germany) and transmission electron microscopes (Philips EM 301). Different methods exist[3] for the determination of the nonstoichiometry of $Zn_{1+\delta}O$. During the present study, the stoichiometric deviation (δ_{Zn}) was measured with good accuracy (~0·1 ppma) and

Table 1. Designation of chemically-prepared ZnO powders

Precursor	*Designation of samples annealed at:*				
	300°C	*500°C*	*700°C*	*900°C*	*1100°C*
$Zn_2(OH)_2CO_3$	ZC300	ZC500	ZC700	ZC900	ZC1100
$Zn_3(OH)_4(NO_3)_2$	ZN300	ZN500	ZN700	ZN900	ZN1100
$ZnC_2O_4 . H_2O$	ZO300	ZO500	ZO700	ZO900	ZO1100

reproducibility (= ±0·3 ppma), using the electrochemical method (coulometric) with modifications following Hagemark and Toren.[17] This method essentially involved the measurement of current resulting from the oxidation of excess Zn, given as:

$$Zn_{1+\delta}O + H_2SO_4 \rightarrow ZnSO_4 + \delta(Zn^{2+} + 2e^-) + H_2O \quad (1)$$

The δ_{Zn} was calculated as:

$$\delta_{Zn} = \frac{M.I.t}{(W_{ZnO}).n.F} = \frac{81{\cdot}36 \times Q \times 10^6}{(W_{ZnO}) \times 2 \times 96{\cdot}5} \text{ ppma} \quad (2)$$

where M is the molecular weight of ZnO; I is the current; t is time; W_{ZnO} is the sample weight; n is the atomic valence number; F is the Faraday constant; and Q is the total charge in coulombs.

The photoluminescence spectra were recorded using a Hitachi 650–60 fluorescence spectrometer containing a solid sample-holder. The reflectance spectra in the UV-visible range were recorded with a Shimadzu UV 210 A double beam spectrometer. The electron paramagnetic resonance (EPR) spectra were recorded using a Varian X-band spectrometer having TE_{011} cavity in the range of 78–300 K. The current–voltage (I–V) characteristics were measured both in d.c. and a.c. mode for the lower current regions (< 10 mA) with a home-built voltage source and a curve tracer. For I–V measurements at higher current values, a d.c. pulse generator producing 8 × 20 μs wave shape together with an oscilloscope was used.

2.3 Processing of ZnO ceramics

Better varistor characteristics have been observed[18] only when the additives used are oxygen-rich compounds of transition metal elements in higher valence states together with the presence of larger ionic-size elements such as $BaCoO_{3-x}$. Pre-annealed ZnO powder was mixed with different amounts of the additive by wet-milling in Teflon-lined ball mill containing plastic balls for 4–6 h in ethanol + acetone mixture. The solvent contained ~0·1% polyvinyl alcohol as the binder. The dry powder was sifted through a nylon mesh. The powder-mix was pelletised at 100 MPa to yield green density in the range 62–68%. The discs were pre-fired at 900°C. This was followed by sintering at selected temperature in the range 1070–1350°C for 1–4 h duration. The sintered ceramics were cooled at a desired rate which varied from 1 to 50°C/min. The sintered discs were 12 mm in diameter and 0·5–1·5 mm thick. Both the faces of the discs were polished with graded alumina, down to 0·3 μm surface-finish, using a polishing machine (Metals Research, Hertfordshire, UK) and subsequently cleaned in an ultrasonic tank. Ohmic contacts were provided by the electroless coating of silver, which was further recrystallised around 250°C.

3 Results

3.1 X-ray line-broadening analysis

All three precursors are annealed from 300 to 1100°C at intervals of 200°C. Typical broadening of the (100) and (002) peaks of 900°C annealed samples are shown in Fig. 1. The corresponding Williamson–Hall plot is shown in Fig. 2. The nonzero slopes of the plot for the ZN900 and ZO900 powders indicate the presence of lattice strain.

Considerable differences exist in the characteristics of the powders depending upon the nature of the precursor. X-ray line-broadening analysis of (100), (300), (002) and (004) peaks have been carried out for the powders annealed at different temperatures. Typical results of the 500 and 900°C annealed samples are shown in Table 2. For all the three routes of preparation, the particle size increases with the temperature of annealing. The ZO300 powder showed the lowest particle size and maximum strain value. As the annealing temperature was raised, the strain value decreased whereas the particle size increased. For the ZO powders, the particle size increases from ~17 nm at 300°C to 30 nm at 900°C. For all three sets of powders, the particle size enhances considerably, when taken to >900°C.

Nearly comparable characteristics were noticed for the ZN powders. The particulate properties for

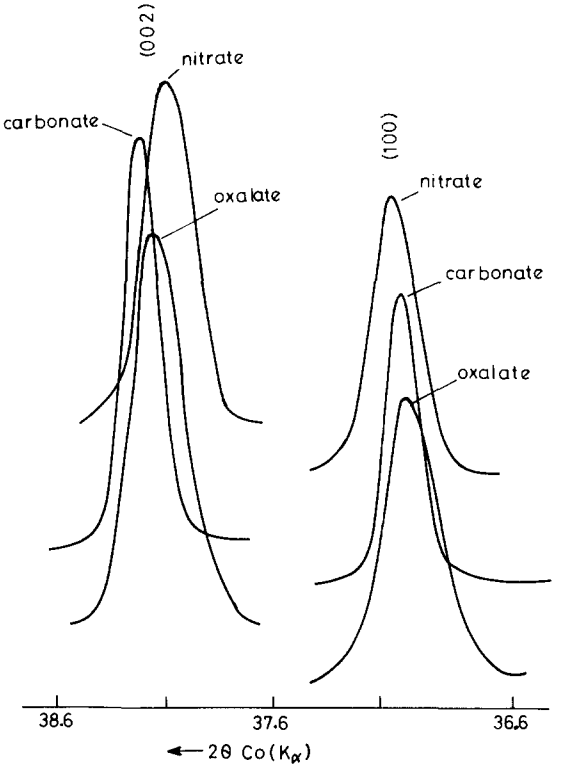

Fig. 1. X-ray diffraction traces of (100) and (002) peaks of ZnO from different routes of preparation and annealed at 900°C.

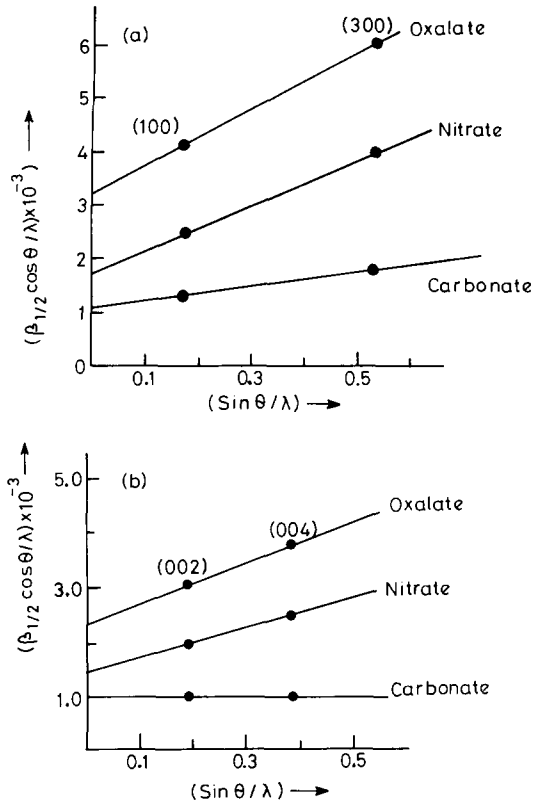

Fig. 2. Typical Williamson–Hall plots of ZnO from the three different routes of preparation annealed at 900°C, using (a) (h00)-type reflections and (b) (00l)-type reflections.

the samples annealed at low temperatures (< 600°C) agree with that reported by Louer *et al.*[19] At higher temperatures of annealing (> 700°C), these authors have observed tremendous increase in particle size. However, the present results showed that up to 900°C of annealing, the particle size for the ZN sample is ≃ 55 nm and increased perceptibly only above 1100°C. The lattice strain decreases with increase in temperature of annealing (Table 2). ZnO obtained from the carbonate precursor showed interesting behaviour. As-prepared and lower temperature (< 700°) annealed samples show less strain compared to other routes of preparation. The particle size is higher than those of ZnO obtained from other routes. As the annealing temperature is increased to ~900°C, the lattice strain becomes negligible, yet the X-ray patterns show broadening due to size effect. The particle size is in the range of 80–100 nm.

3.2 Analyses by microscopy

The ZN powders showed strong agglomerating tendency, irrespective of the annealing temperature. Optical micrographs of ZN500 samples show agglomerate size of 60–80 μm and the agglomerative character is retained even after annealing at 900°C (Fig. 3(a)). ZO900 powders, on the other hand, are fine-grained (Fig. 3(b)). They also show weak agglomeration but the average agglomerate size is far smaller than that of the ZN powders.

The ZC powders showed entirely different behaviour. ZC500 samples retained the same morphology and size of the precursor carbonate and had an agglomerate size ~ 150 μm. However, ZC900 exhibited individual crystallites of ~0·1 μm (Figs 3(c) and (d)) which nearly agrees with the X-ray size value. The shape of the individual particles remained nearly cylindrical.

3.3 Nonstoichiometry of ZnO

3.3.1 Electrochemical analysis

The most important parameter which considerably influenced the reactivity and the electrical properties of the final ceramics is the nonstoichiometry of the starting $Zn_{1+\delta}O$ powder. Typical plots of the electrochemical current, as a function of time, for the ZC powders are shown in Fig. 4. The δ_{Zn} values of powders annealed at different temperatures are shown in Table 3. The stoichiometric ZnO contains $4{\cdot}21 \times 10^{22}$ Zn atoms/cm^3 and hence 1 ppma corresponds to $4{\cdot}21 \times 10^{16}$ atoms/cm^3. The ZO300 and ZO500 powders always showed tremendously larger δ_{Zn} values (Table 3). The ZN300 and ZN500 powders have slightly higher δ_{Zn} values, as compared to the ZC powders. With increase in temperature of annealing, the ZN and ZC powders showed increase in the δ_{Zn} value. Although ZO powders exhibited

Table 2. Crystallite size and lattice strain of ZnO powders, from Williamson–Hall plot

Precursor	*Decomposition temp. and time*	*(100) and (300)*				*(002) and (004)*				$f_C = (H_C/D_C)$	$f_G = (H_G/D_G)$
		$e_C \times 10^{-3}$	$e_G \times 10^{-3}$	D_C (nm)	D_G (nm)	$e_C \times 10^{-3}$	$e_G \times 10^{-3}$	H_C (nm)	H_G (nm)		
Nitrate		1·7	2·0	40	36	1·4	1·6	57	55	1·42	1·52
Carbonate	500°C–12 h	0·8	0·9	67	62	0·5	0·7	79	74	1·18	1·19
Oxalate		1·9	2·1	22	20	1·5	1·8	33	28	1·50	1·40
Nitrate		1·0	1·1	54	51	0·7	0·9	69	63	1·27	1·23
Carbonate	900°C–12 h	0	0	78	76	0	0	100	96	1·28	1·26
Oxalate		1·3	1·6	31	28	0·9	1·0	42	40	1·35	1·43

e_C, Cauchy strain; e_G, Gaussian strain; D_C, Cauchy mean crystallite size; D_G, Gaussian mean crystallite size; H_C, average Cauchy height perpendicular to (001)—type plane; H_G, average Gaussian height perpendicular to (001)—type plane; f_C, Cauchy shape factor; f_G, Gaussian shape factor.

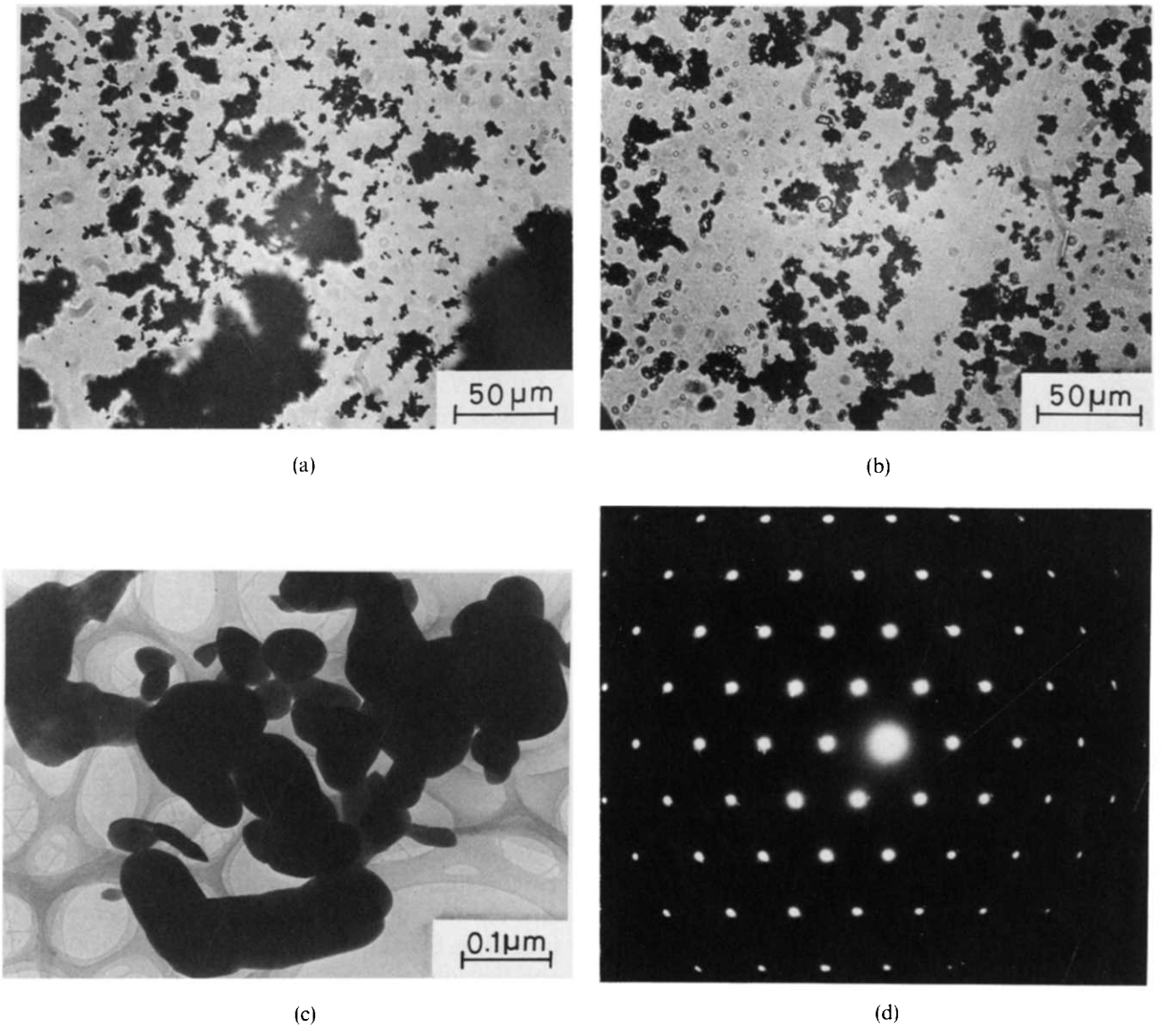

Fig. 3. Optical micrograph of (a) ZN900 and (b) ZO900 powders. (c) and (d) are the TEM micrograph of ZC900 and its corresponding diffraction pattern.

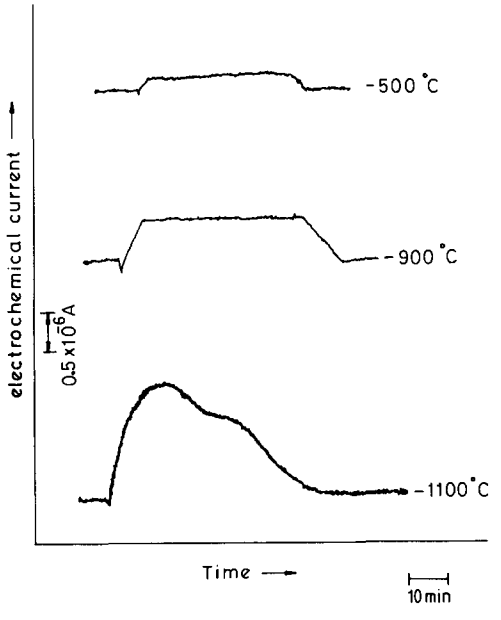

Fig. 4. Typical plots of electrochemical current versus time for the ZC powders annealed at different temperatures.

highst δ_{Zn} at lower temperatures, with increase in temperature of annealing, δ_{Zn} decreased and became negligible at 900°C. With further increase in temperature, δ_{Zn} again started increasing (Table 3).

3.3.2 Optical properties

Optical properties of ZnO also showed tremendous difference with respect to the nature of the precursor. The ZN300 and ZC300 powders are white in colour. With increase in temperature of annealing, these powders become light yellow in colour. The yellow coloration increases with the temperature of annealing. When treated in oxygen at 600–700°C, the powders turn white. The reflectance spectrum of the ZC powders, treated at different temperatures, are shown in Fig. 5(I). With increase in temperature of annealing, the absorption edge shifts to higher wavelength. This red-shift in the absorption edge is proportional to the yellow coloration and is found to be proportional to δ_{Zn} values. After annealing in

Table 3. Excess Zn levels for ZnO annealed at different temperatures

Precursor	*Annealing temp.*	δ_{Zn} (*ppma*)
Nitrate		3·5
Carbonate	500°C	1·8
Oxalate		25·0
Nitrate		11·3
Carbonate	900°C	8·6
Oxalate		0·5
Nitrate		15·0
Carbonate	1100°C	12·8
Oxalate		2·4

O_2, the absorption edge reverted back. Similar behaviour was observed for the ZN powders. The ZO powders showed differences. ZO300 showed the absorption edge at higher wavelength compared to the preparation from other routes. With increase in annealing temperature, it shifted to lower wavelength.

3.3.3 Photoluminescence

The ZC300 and ZC500 powders showed very weak luminescence in the yellow-orange region, possibly due to the presence of Mn^{2+} impurities. These weak luminescences were observed at the precursor stage itself for the carbonate under UV excitation. With increase in temperature of annealing (900°C), the weak luminescence shifted to the blue-green region. For the ZO500 powder, intense broad green emissions, centred at 530 mm were observed (Fig. 5(II)). With further increase in the temperature of annealing, the spectral intensity decreased and became negligible at 900°C. When annealed in a neutral atmosphere (Ar), the luminescence intensity was preserved.

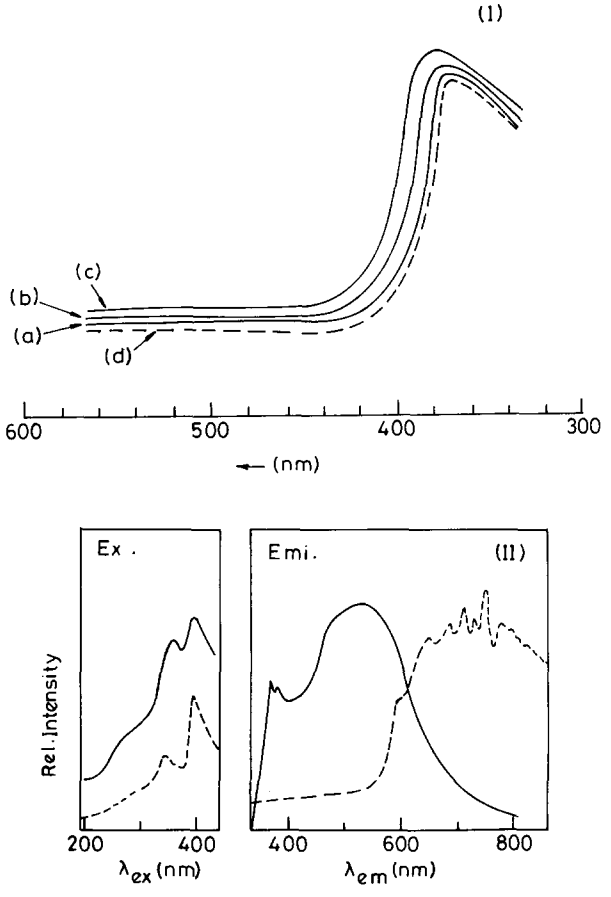

Fig. 5. Reflectance spectrum of (a) ZC500, (b) ZC900 and (c) ZC1100. (d) ZC powder annealed in oxygen at 700°C. (II) The excitation and emission spectrum of ZC500 (dashed line) and ZO500 (solid line).

3.3.4 EPR results

It is well known[20] that ZnO exhibits a donor-type EPR-signal at $g \sim 1{\cdot}956$ and this signal has been variously attributed to $V_O^{\cdot}$, $Zn_i^{\cdot}$ or to the conduction band electrons. After careful analysis with respect to O_2 annealing and donor addition, the authors have assigned[21] this signal to $V_O^{\cdot}$ with superhyperfine interactions with the cations at the nearest neighbour sites. Figure 6 shows the variation in the intensity of this signal with temperature of annealing for the various routes of preparation. The intensity of this signal was less for the ZC300 samples and slightly increased for the ZN300 samples. However, the ZO300 sample exhibited the maximum intensity for this signal. Both the ZN and ZC powders have increased intensity for this signal, as the annealing temperature is increased, whereas the ZO powders showed the inverse trend with temperature of annealing. For the ZO900 sample the signal intensity was the lowest, which indicated an upward trend with further increase in annealing temperature. Under neutral or reducing atmosphere of annealing, the ZO powders retained higher intensity even at ~900°C.

3.4 Sintering behaviour

Sintering behaviour of ZnO is considerably dependent upon the route of preparation and the kind of

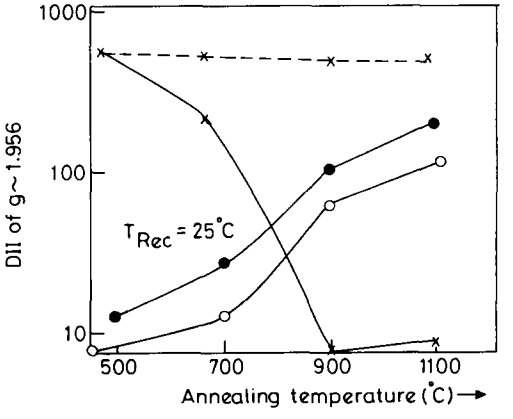

Fig. 6. Variation of the intensity of $g \sim 1{\cdot}956$ signal with temperature of annealing. Nitrate (●), carbonate (○) and oxalate derived (×) ZnO. Oxalate derived ZnO annealed in Ar atm. (----).

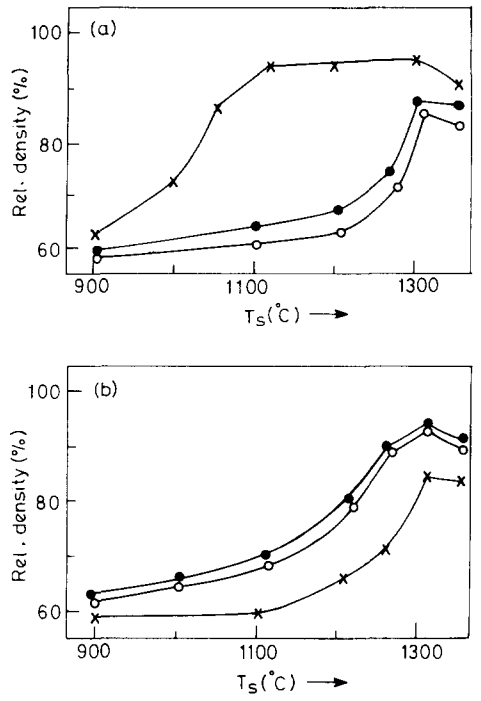

Fig. 7. Densification of ZnO as a function of sintering temperature for ZnO powders from different route of preparation annealed at (a) 500 and (b) 900°C. (○) Carbonate, (●) nitrate and (×) oxalate derived ZnO.

pre-treatment to which the powders have been subjected. For the 500°C annealed powders, the densification (in the absence of any additives) as a function of sintering temperature (duration = 2 h) is given in Fig. 7(a). The ZO500 powder was highly reactive and started sintering at comparatively lower temperatures (1050°C). The discs attained maximum relative density (~95%) at ~1120°C and remained nearly constant with further increase in temperature. Both the ZC500 and ZN500 samples were less reactive and sintering begins only above 1250°C. The maximum density attained was only ~85% at 1300°C. The ZN powders showed slightly higher density, compared to the ZC powders at any given temperature of sintering. When $T_{sinter} > 1320$°C, the density started decreasing in all the cases.

Figure 7(b) shows the densification curves for the 900°C annealed powders without any additives at different sintering temperatures with 2 h as the sintering duration. The ZC900 and ZN900 powders showed better sintering characteristics. The densities attained at a given sintering temperature are higher than those of the 500°C annealed samples. In the case of ZO900, the behaviour is different. It required higher temperature of sintering compared to the 500°C annealed samples. The density attained at a given temperature for ZO900 was less than that attained by powders obtained through the other routes of preparation. With powders annealed at 1100°C, the densities were less compared to the samples annealed at 900°C, irrespective of the preparation route. This may be due to the increased particle size which overrides the effect of nonstoichiometry on the reactivity of the powders.

In order to study the effect of additives on the sintering behaviour, 1 mol% $BaCoO_{2.96}$ was taken along with the pre-annealed zinc oxide powders. The additive was mixed with ZnO and sintered at different temperatures for 2 h. The extent of shrinkage as a function of sintering temperature is plotted in Fig. 8(a). ZO500 showed maximum shrinkage at 1100°C itself. With further increase in sintering temperature, the shrinkage remained nearly constant. Using ZN500 and ZC500 powders, maximum shrinkage is observed only at 1300°C. The magnitude of shrinkage is less for these two routes of preparation, compared to the oxalate route. The shrinkage diminishes when taken to above 1300°C.

When the powders were annealed at 900°C and then mixed with 1 mol% $BaCoO_{2.96}$, the sintering behaviour differed. Both ZN900 and ZC900 powders showed maximum shrinkage at 1100°C itself. On the other hand, the ZO900 powder was less reactive and attained less shrinkage even at 1300°C (Fig. 8(b)).

Since ZO500, ZN900 showed higher δ_{Zn} values, as well as lower particle size, the sinterability is higher with these powders. At lower temperatures (<1100°C), the sintering is determined by the out-diffusion of Zn ions or of oxygen vacancies and formation of ZnO at the surface.[22] At higher temperatures (>1300°C) the density again starts

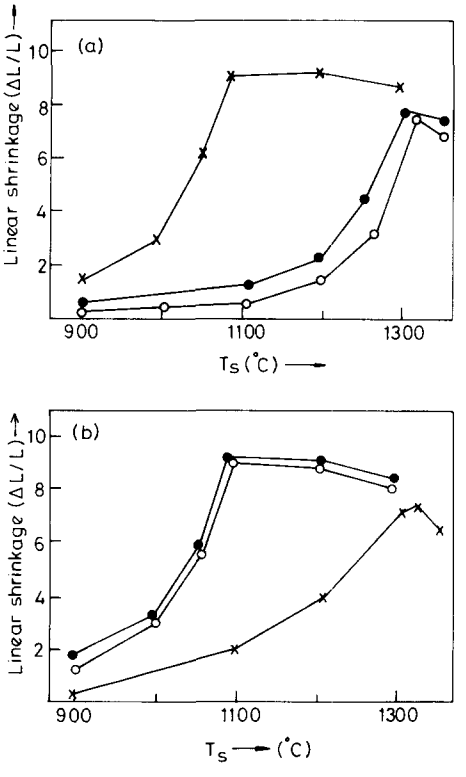

Fig. 8. Linear shrinkage as a function of temperature for ZnO sintered with 1 mol% $BaCoO_{2.96}$ with (a) 500 and (b) 900°C annealed ZnO powders. Carbonate (○), nitrate (●) and oxalate derived (×).

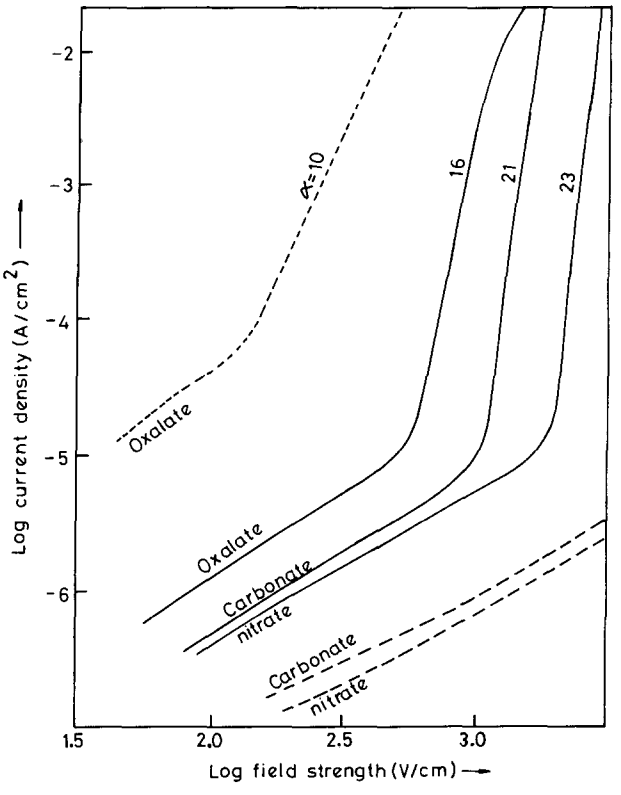

Fig. 9. *I–V* characteristics of 1 mol% $BaCoO_{2.96}$ ceramics with ZnO obtained through different routes and annealed at 500°C (dashed line) and 900°C (solid line).

decreasing, indicating the evaporation of ZnO as the material transport mechanism.[22]

3.5 Effect of different routes of preparation on the electrical properties

The *I–V* characteristics of ZnO prepared from the three routes of preparation were studied with 1 mol% $BaCoO_{2.96}$ as the additive. Pellets were sintered under identical conditions at 1100°C for 2 h and were fast-cooled (50°C/min).

Figure 9 shows the *I–V* relations obtained for the 500 and 900°C annealed powders. For the 500°C annealed powders, only the ZO powders showed measurable nonlinearity. Both ZN500 and ZC500 showed linear *I–V* relations. For the 900°C annealed ZnO, all the three routes of preparation exhibited nonlinearity. The ZO900 powder showed higher leakage current and lower breakdown voltage. The nonlinear range is shorter, i.e. the upturn region is observed at lower current densities, in the case of ZO900; ZC900 and ZN900 powders showed comparable nonlinearity. The leakage current remained almost similar but the nitrate derived sample showed higher breakdown voltage.

4 Discussion

In the temperature ranges of ZnO formation from the precursors, equilibriation of the point defects in accordance with the thermodynamic characteristics is not possible. This is because the mobility of lattice defects is kinetically restricted at lower temperatures. Therefore, the defect contents greatly depend upon the nature of the formation reaction(s). Strongly exothermic oxalate decomposition generates reductive atmosphere of $CO + CO_2$ and the heterogeneous back reaction of the evolved gases leads to the disproportionation of part of CO to $C + CO_2$. This is evident from the carbon deposited on the powders when the decomposition is carried out in a vacuum or under an inert atmosphere. Oxidation of carbon leads not only to the removal of oxygen ions but also imparts electrons to the powder particles. Therefore, the native defect concentration in the particles is much higher than the thermodynamic equilibrium values, a fact which is supported by the EPR results. Internal strain is produced by the change in composition, lattice structure as well as by the thermal gradient during the formation of the ZnO particles from the precursors. Increase in strain is also possible because of the aggregation of vacancies present in high concentration or from the carbon deposited. Since the structural coherence, the thermal gradient (depending upon the magnitude of heat change and the exo- or endothermic nature) and also the back reaction from the evolved gases vary with the precursor, the residual strain in the resultant powders differ considerably. As the annealing temperature is increased, the lattice strain decreases and, more importantly, the mobility of the point defects enhances. Thus, the oxygen vacancies present in excess of the equilibrium values are annihilated because of the out-diffusion of these defects and hence δ_{Zn} decreases with increasing temperature for the ZO powders. This can be effectively faster because of the small particle size. The carbonate decomposition produces a neutral atmosphere and hence the nonequilibrium amount of point defects produced will be low. Furthermore, because of the weakly endothermic nature of the decomposition, the thermal gradients are small and hence the strain values are less compared to the other two routes of preparation. The nitrate decomposition produces oxidative atmosphere by way of $NO + NO_2$ and hence the low value of δ_{Zn} for the as-decomposed samples. However, because of the highly exothermic nature of this decomposition and hence the larger thermal gradients, the lattice strain and the δ_{Zn} values are higher than those of the powders from the carbonate route. Structural coherence, at least on certain specific crystallographic directions, allows for lower lattice strains which is the case for the carbonate derived powders. Thus, ZC500 powders retain the same morphology and the agglomerate character as of the precursor carbonate. However, calcination above 900°C leads

to the break up of agglomerate to individual crystallites, thereby lowering the effective particle size. As the annealing temperature is increased (particularly $\geq 900°C$), more and more equilibrium point defects are created and hence the δ_{Zn} as well as the EPR signal intensity at $g \sim 1{\cdot}956$ increases. The particle size, the concentration of δ_{Zn} as well as the presence of lattice strain considerably affect the reactivity (and hence the sinterability) and consequently the performance of the device. The ZO500 powders have low particle size as well as higher δ_{Zn} concentration. Thus, the reactivity of these powders is high and hence they could be sintered at comparatively lower temperatures. Better sintering characteristics of this powder even in the presence of additives lead to the nonlinearity in the corresponding ceramics. Even though the particle size of ZN500 is comparable to that of ZO500 powders, the δ_{Zn} values are very low in the former and hence the sinterability and therefore the final electrical characteristics are poor.

As the ZO powders are annealed at higher temperatures, the particle size increases accompanied by the drastic decrease in δ_{Zn} and the intensity of the EPR signal at $g \sim 1{\cdot}956$. Hence, the sintering and the electrical characteristics of higher temperature annealed ZO powders are poorer. In the case of ZN and ZC powders, annealing at higher temperatures brings in more defect concentration. Hence, the sinterability of ZC900 and ZN900 has improved.

The importance of the nonstoichiometry of ZnO powder and that of the oxidative additives in the varistor forming mechanism has already been dealt with by the authors in Ref. 18. The oxidised form of the nonstoichiometric additive phase *in situ* produces oxygen, as the sintering temperature is approached. The native donor states already present in ZnO particles as a result of nonstoichiometry provide the favourable energy levels for the chemisorption of thermally released oxygen (Fig. 10). The electrons are trapped by the adsorbed oxygen to form negatively charged surface states, so as to produce the depletion layer. The space-charge region is preserved during sintering because of the higher valence state of the transition metal ions. In turn, the high valent transition metal ion impurities are charge-compensated by the cation vacancies. The holes from the valence band may find their way to the surface states, being mediated by the acceptor levels arising out of the cation vacancies (Fig. 10(b)). This means that even when the adsorbed oxygen is released as neutral species, the depletion layer will be preserved.

Because of the impeded grain growth, the ZN ceramics show higher breakdown voltage as compared to the ZC samples. Even though ZO900 samples show

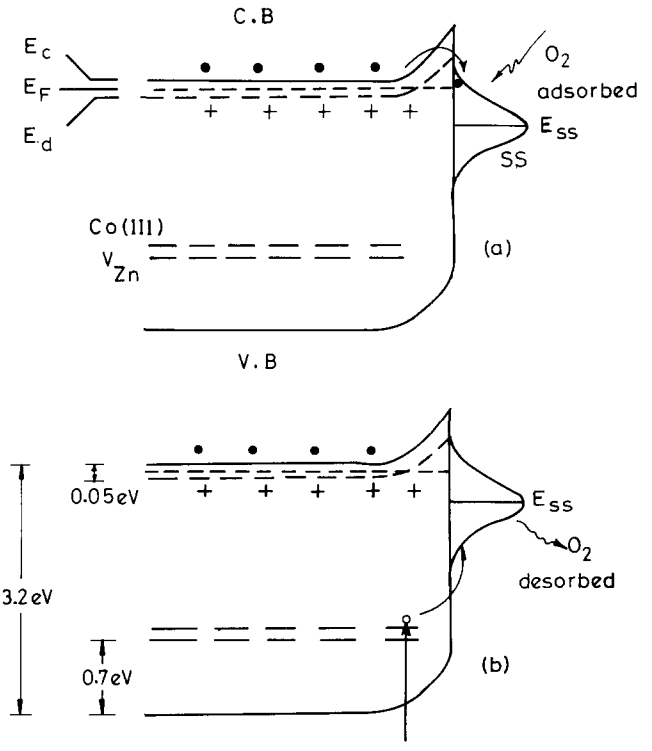

Fig. 10. Band model for the varistor forming mechanism: (a) chemisorption of oxygen and the formation of depletion region near the grain boundary; (b) neutralisation of oxygen by the hole and its desorption.

nonlinear action, the upturn occurs at lower current density region because of the decrease in the δ_{Zn} value and hence the higher grain core resistivity. Annealing the powders at still higher temperatures ($> 1000°C$) increases the particle size and decreases the reactivity of the particles as evident from the lowered sinter density. Although ZO500 powder exhibits lower particle size and good reactivity, the δ_{Zn} values are higher than the optimum and hence the leakage current is very high. Besides this the nonlinearity is less compared to the ZN900 and ZC900 samples. Both ZN900 and ZC900 samples show comparable nonlinearity indices and comparable leakage currents. However, the ZN900 samples are fine-grained and hence are useful in high voltage applications, whereas, for the low-voltage electronic circuit applications, ZC900 samples are more suitable.

5 Conclusions

The present results show that the critical concentrations of the point defects of the starting powders rather than the particle size are better correlatable to the nonlinear resistivity of the final ceramics. The results from the X-ray line broadening analysis show maximum lattice strain for ZN300 and ZO300, whereas the ZO300 powders tend to be more agglomerative. The extent of nonstoichiometry is influenced by the back reaction of the evolved gases.

The δ_{Zn} value of ZO300 powders (25 ppma) is far off from the equilibrium value. The influence of the gaseous products on the nonstoichiometry is also evident from the lower δ_{Zn} values for the ZC300 and ZN300 powders. Furthermore, with increasing annealing temperature, the δ_{Zn} decreases for the oxalate derived sample, whereas the reverse trend is observed in nitrate and carbonate derived powders. If the particle size alone was the decisive factor in the formation of nonlinear resistors, ZO300 followed by ZN300 should have given better results, which is not the case. A very low δ_{Zn} value, as in the case of ZC300 or ZO900, is also inadequate to give higher nonlinearity.

References

1. Heiland, G., Mollwo, E. & Stockmann, F., *Sol. Stat. Phys.*, **8** (1959) 191.
2. Brown, H. E., *Zinc Oxide—Properties and Applications*. International Lead and Zinc Research Organization, New York, 1976.
3. Hirschwald, W., In *Current Topics in Materials Science, Vol. 7*, ed. E. Kaldis. North-Holland, Amsterdam, 1981, p. 148.
4. Suyama, Y., Tomokiyo, Y., Manabe, T. & Tanaka, E., *J. Am. Ceram. Soc.*, **71** (1988) 391.
5. Dupont-Pavlovsky, N., *Phys. Stat. Sol.*, **A35** (1976) 615.
6. Narayana, D., *J. Phys. Chem.*, **74** (1970) 779.
7. Klissurski, D., Uzunov, I. & Kumbilieva, K., *Thermo Chimica Acta*, **93** (1985) 485.
8. Auffredic, J. P. & Louer, C., *Reactivity of Solids*, **4** (1987) 105.
9. Barring, E. A., Bruce, F. M. & Kent, B. H., US Patent No. US 4 543 341, 24 Sept. 1985.
10. Josef, V. *et al.*, Czech. Patent No. 217 926, 15 Dec. 1984.
11. Fischer, C., *Z. Chemie*, **13** (1973) 66.
12. Lauf, R. J. & Bond, W. D., *Ceram. Bull.*, **63** (1984) 278.
13. Revathi, R., PhD thesis, Blue emitting A.C. electroluminescent $Zn_{1-x}Mg_xS$:Cu,Br powder phosphors. Indian Institute of Science, Bangalore, India, 1986.
14. Klug, H. P. & Alexander, L. E., *X-Ray Diffraction Procedures For Polycrystalline and Amorphous Materials* (2nd edn). John Wiley, New York, 1974, p. 625.
15. Warren, B. E. & Averbach, B. L., *J. Appl. Phys.*, **23** (1952) 1959.
16. Rachinger, W. A., *J. Sci. Inst.*, **25** (1948) 253.
17. Hagemark, K. I. & Toren, P. E., *J. Electrochem. Soc.*, **122** (1975) 992.
18. Raghu, N. & Kutty, T. R. N., *Appl. Phys. Lett.*, **60** (1992) 100.
19. Louer, D., Vargas, R. & Auffredic, J. P., *J. Am. Ceram. Soc.*, **67** (1984) 136.
20. Neumann, G., In *Current Topics in Materials Science, Vol. 7*, ed. E. Kaldis, North-Holland, Amsterdam, 1981, p. 267.
21. Kutty, T. R. N. & Raghu, N., *Mat. Sci. & Engg*, **13B** (1992) 181.
22. Kobayashi, K., Dordor, P., Bonnet, J. P., Salmon, R. & Hagenmuller, P., *J. Mat. Res.*, **2** (1987) 478.